Int. J. Peptide Protein Res. **44**, 1994, 388–398
Printed in Belgium – all rights reserved

INTERNATIONAL JOURNAL OF
PEPTIDE & PROTEIN RESEARCH
ISSN 0367-8377

^{1}H NMR analysis of fibril-forming peptide fragments of transthyretin

JACQUELINE A. JARVIS[1], ALAN KIRKPATRICK[2] and DAVID J. CRAIK[1]

[1] *School of Pharmaceutical Chemistry, Victorian College of Pharmacy, Monash University, Parkville, Victoria, Australia and*
[2] *CSIRO Division of Biomolecular Engineering, Parkville, Victoria, Australia*

Received 24 November 1993, accepted for publication 2 April 1994

Peptide fragments of the protein transthyretin, previously shown to form cross β-sheet amyloid-like fibrils *in vitro*, were investigated using ^{1}H 1D and 2D NMR techniques. TTR 10–20, TTR 105–115 as well as a substituted analogue, (TTR 105–115^{Met111}) all formed amyloid-like fibrils readily in 20–30% acetonitrile/water at room temperature. It was found that the presence of fibrils in the peptide solutions did not affect the observable NMR spectra, which may have been due to the line-broadening that would be associated with these macromolecular species. ^{1}H NMR spectra were thus representative of the monomeric form of the peptide in solution. Information from D_2O exchange, $^3J_{NH-\alpha H}$ coupling measurements, temperature coefficients and NOESY experiments suggested that these peptides have some propensity for turn or helix but were predominantly unstructured. There was no indication of the monomeric species existing predominantly in an extended form, suggesting that the formation of β-sheet based fibrils does not require preformed extended structures. TTR 105–115^{Met111} displayed slight structural differences from TTR 105–115 which may be related to the fibril-forming propensity of the corresponding mutant TTR. © Munksgaard 1994.

Key words: amyloid fibril; nuclear magnetic resonance; peptide; TTR

Transthyretin (TTR) is a 55 kDa protein which serves as a serum carrier of thyroid hormones as well as retinol binding protein (RBP) and retinol. The protein is made up of four identical 127 residue monomers, and its three-dimensional structure has been characterised to 1.8 Å using crystallographic techniques (1). TTR, some TTR fragments and variant TTR have a propensity to form amyloid fibrils which are associated with familial amyloidotic polyneuropathy (FAP) and senile systemic amyloidosis (2–4). In these disorders the fibrils form insoluble deposits which interfere with normal tissue or neuron function, ultimately resulting in death. This generalised phenomenon has also been implicated in several other disease states, including rheumatoid arthritis, type II diabetes, Alzheimer's disease and specific polyneuropathies (5, 6). The study of amyloidosis therefore has important implications for a broad range of therapy development.

The structural basis for the formation of the amyloid fibril is, at present, poorly understood. Electron microscopic studies have demonstrated that amyloid deposits are typically composed of massive arrays of twisted, non-branching fibres, approximately 10 nm in diameter, and of indeterminant length. This morphology and the characteristic green birefringence of fibrils upon staining with congo red have been interpreted in terms of an antiparallel β-sheet based structure. In the generally accepted model, derived from X-ray diffraction data, β-sheets are formed with hydrogen bonding aligned parallel to the fibre axis, and sheets stacked laterally (7–9).

Further investigations have been conducted on synthetic amyloid-like fibrils formed *in vitro*. Several peptides, representing specific regions of the amyloidogenic proteins, have been shown to independently form amyloid-like material. Studies of these systems have provided additional information regarding the kinetics, predisposing conditions and sequence requirements of fibril formation. In particular, circular dichroism (CD), Fourier transform infrared (FTIR) spectroscopy, fluorescence and turbidity studies have been used to determine concentration dependencies and nucleation

Abbreviations: NMR, nuclear magnetic resonance; NOE, nuclear Overhauser enhancement; NOESY, NOE spectroscopy; DQF-COSY, double quantum filtered correlation spectroscopy; TOCSY, total correlation spectroscopy; 1D, one-dimensional; 2D, two-dimensional; TTR, transthyretin; ppm, parts per million; DSS, 4,4-dimethyl-4-silapentane-1-sulfonate; $d_{\alpha N}(i,j)$, $d_{NN}(i,j)$, *etc.*, intramolecular distance between the protons αH and NH, NH and N *etc.*, on residues i and j; TPPI, time-proportional phase incrementation.

properties of fibril formation as well as to confirm the β-sheet nature of the amyloid (10–14). Owing to the poor solubility of such species, however, relatively few of these peptides have been structurally analysed using ^{1}H NMR methods. There is, hence, only a limited understanding of the structural transitions that take place as the monomeric species becomes incorporated into the fibrillar aggregate.

We present the first ^{1}H NMR structural analysis of peptide fragments from the protein transthyretin (TTR), previously reported to form amyloid-like fibrils *in vitro* (15), and shown to possess a cross β-sheet arrangement by X-ray diffraction (16). These include TTR 10–20 and TTR 105–115, representing β-strands A and G, respectively, located in the inner β-sheet region of TTR that forms the thyroid hormone binding site (Fig. 1). A peptide analogue of TTR 105–115 (TTR 105–115^{Met111}) was also examined, since this mutation is known to increase the propensity of TTR to form amyloid (18). It was of interest to determine whether the same substitution in TTR 105–115 would have a structural effect on the peptide or increase the peptide's ability to form fibrils.

MATERIAL AND METHODS

Peptide synthesis and sample preparation

TTR 10–20, TTR 105–115 and TTR 105–115^{Met111} were synthesised on an Applied Biosystems model 430A synthesiser by solid-phase methods using fluorenyl methyloxycarbonyl (Fmoc) chemistry. The resin used for the synthesis was parahydroxymethylphenoxymethyl–polystyrene (HMP). The side-chain protecting groups were trityl (Trt) for Cys, butyloxycarbonyl (Boc) for Lys and tertiary butyl (tBu) for Asp. The cleavage procedure used involved a 90 min treatment of the bound peptide with 95% trifluoroacetic acid, containing phenol, ethane dithiol, thioanisol and water as scavengers.

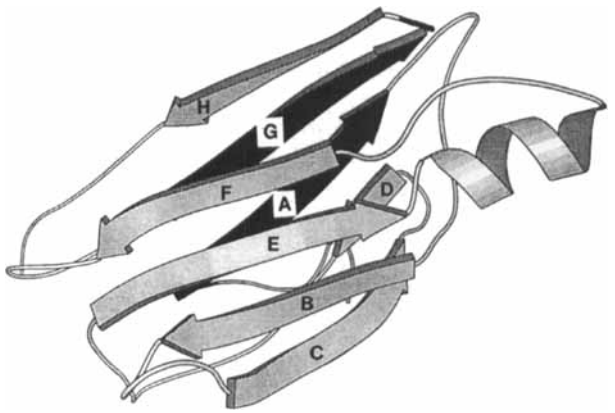

FIGURE 1

Structure of the transthyretin monomer determined by X-ray crystallography (1), showing positions of regions 10–20 and 105–115 in the native TTR structure (A and G strands) (1). The β-strands represent inner-sheet regions that line the central ligand binding cavity. Side-chains are involved alternately in intersheet hydrophobic interactions and in forming the ligand binding contacts. The diagram was drawn using the program Molscript (17).

The amino acid sequences were as follows:

TTR 10–20: Cys-Pro-Leu-Met-Val-Lys-Val-Leu-Asp-Ala-Val

TTR 105–115: Tyr-Thr-Ile-Ala-Ala-Leu-Leu-Ser-Pro-Tyr-Ser

TTR 105–115^{Met111}: Tyr-Thr-Ile-Ala-Ala-Leu-Met-Ser-Pro-Tyr-Ser

The peptides were purified using a Waters radial diffusion reversed-phase cartridge and LC 1500 HPLC system (ICI instruments). Mobile phase A contained 0.01% TFA/H_2O and mobile phase B contained 0.01% TFA/90% acetonitrile/H_2O. A 40 min 10% to 60% B gradient elution was used at a flow rate of 10 mL/min. Amino acid analysis, analytical HPLC and NMR confirmed the purity of the samples. FAB-MS yielded the correct molecular ions (TTR 10–20 MH^+ = 1187.4; calcd 1187.6: TTR 105–115 MH^+ = 1198.3; calcd 1198.6: TTR 105–115^{Met111} MH^+ = 1216.2; calcd 1216.2). Acetonitrile was of HPLC grade (Ajax chemicals). Water was distilled and deionised. Other chemicals were of reagent grade and were used without further purification.

The peptides were insoluble in water, but could be dissolved in millimolar concentrations in solutions of 20–30% acetonitrile/water. It was found that the fibrils formed most readily in solutions of low acetonitrile concentrations. Hence samples for electron microscopy and polarised light microscopy were prepared in 20% acetonitrile solutions. Higher percentages of acetonitrile appeared to slow down the fibril formation (depending also on the peptide concentration), and 30% acetonitrile solutions were therefore employed for NMR studies to avoid the rapid depletion of signal that was anticipated to occur upon fibril formation.

The peptides were made up for NMR experiments in 5 mm tubes (Wilmad) at concentrations varying between 0.5 and 20 mM in (i) 30% acetonitrile solutions and (ii) 30% acetonitrile/D_2O solutions. The pH was left at 3–4. Preparations of cysteine and methionine-containing peptides were degassed with N_2, and the NMR tube was sealed to avoid oxidation of the sulfur groups.

Electron microscopy

10–40 mg/mL solutions of TTR 10–20, TTR 105–115 and TTR 105–115^{Met111} were dissolved in 20% acetonitrile. The samples were kept at room temperature and examined the next day and several weeks later by transmission electron microscopy. Aliquots for electron microscopy were placed on butvar-98-coated copper or nickel grids and negatively contrasted with 2% uranyl acetate. Transmission electron microscopy was conducted on a Jeol 100S instrument.

Polarised light microscopy
Aliquots of the gel formed from peptide solutions were air dried on glass slides for 2 min with 80% ethanol, and stained for 5 min with 5% congo red prepared in ethanol saturated with NaCl (19). Excess congo red was removed by washing with 90% ethanol. The stained samples were examined for green birefringence using a WILD M32 light microscope equipped with polarising lenses, optimally aligned with respect to the sample.

NMR experiments
^{1}H NMR spectra were recorded on Bruker AMX 300 and 500 MHz spectrometers using time-proportional phase incrementation for quadrature detection in the f_1-dimension (20). The water proton signal was suppressed by low-power irradiation during the relaxation delay (1.5 s) and during the mixing time of NOESY experiments. Low-temperature studies employed a thermostat controlled stream of cooled air (Haake SK 107). Spectra were referenced internally using 4,4-dimethyl-4-silapentane-1-sulfonate (DSS).

One-dimensional spectra were recorded at 5 °C increments at 300 MHz over a temperature range of 25–45 °C, over 16384 data points. Temperature coefficients for the chemical shifts of the amide protons were measured primarily from these spectra. $^3J_{NH-\alpha H}$ coupling constants were measured from both 1D spectra and DQF-COSY experiments. Spectra run in D_2O solutions were used to monitor the exchange of NHs, and TOCSY spectra used to confirm the assignments of slower exchanging peaks.

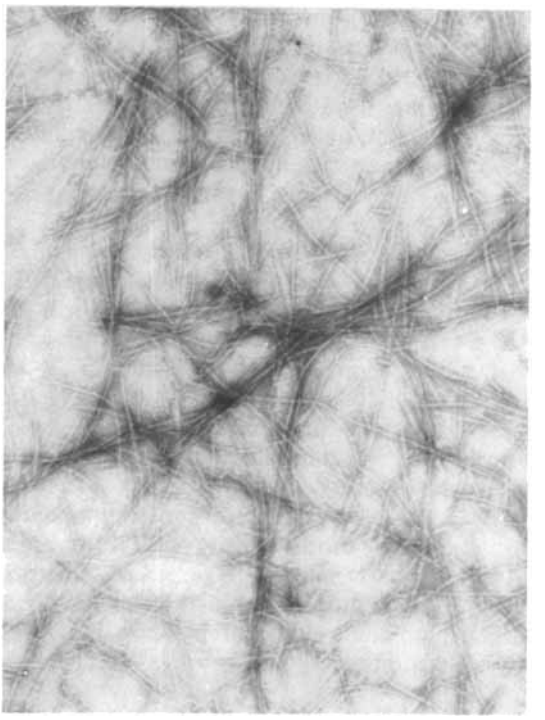

FIGURE 2
Electron micrographs of fibrillar structures formed by TTR 105–115 in 20% acetonitrile/water (×40000).

TOCSY experiments were recorded using an MLEV-17 mixing scheme (21). Mixing times of 120 ms

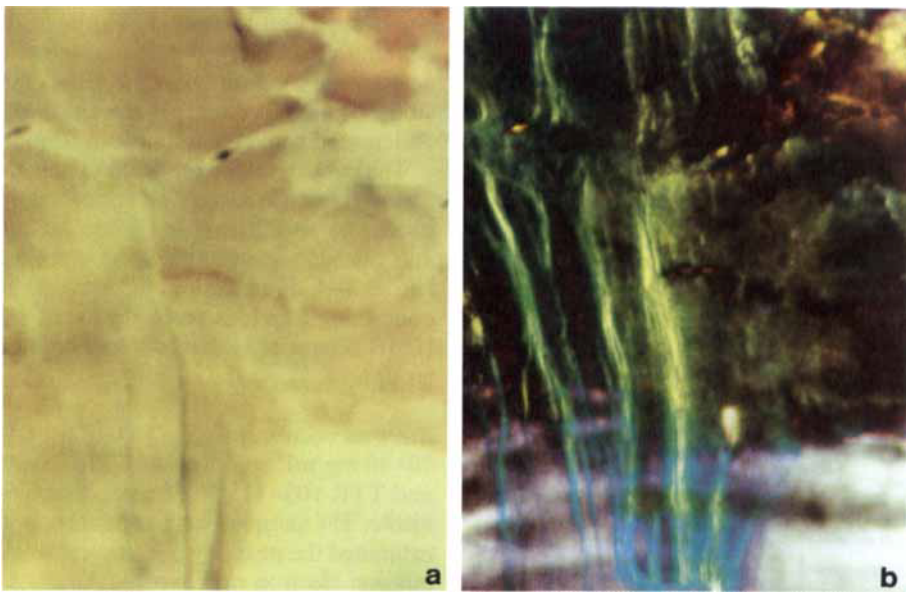

FIGURE 3
Light micrographs of a gelled peptide sample stained with congo red: (a) under normal lighting and (b) under plane polarised light (×40). The purple red colouration is due to the congo red stain, and the green gold appearance of the sample under polarised light is evidence of massive fibril formation.

were used, which enabled all intraresidue connectivities to be observed. Double quantum filtered (DQF)-COSY experiments (22) were used in the assignment process and were also used to measure $^3J_{NH-\alpha H}$ coupling constants. 2 s delays were employed for these experiments to allow relaxation between pulses. NOESY experiments were acquired at 500 MHz at 1 °C. NOESY experiments employed a jump-return pulse (23) in place of the final 90 ° pulse in the sequence to avoid excitation of the water resonance, as well as very mild presaturation.

2D experiments were collected over 4096 complex data points at 500 MHz. Usually 512 increments of 32 scans were acquired over a spectral width corresponding to 10 ppm for both dimensions. Up to 64 scans per increment were acquired for less sensitive NOESY experiments, and only four scans per increment were required for diagnostic TOCSY experiments. Up to 800 increments were collected for improved resolution in the t_1-dimension in the DQF-COSY and NOESY experiments.

The data were processed on a Silicon Graphics (SGI 4D/30) computer using the Felix version 1.0 software package (Hare Research, Inc). The t_1-dimension was zero-filled to 4096 real data points, with both dimensions being multiplied by a sine bell function shifted by 90 ° prior to Fourier transformation. Polynomial baseline correction in selected regions also improved the appearance of the spectrum.

NOE crosspeak intensities were classified as strong, medium or weak according to their relative volumes measured in Felix.

RESULTS

Fibril formation

For the NMR and fibril formation studies, TTR 10–20, TTR 105–115 and TTR 105–115^{Met111} were prepared in water or D_2O to which d_3-acetonitrile was added to assist solubility. It was found that 20% acetonitrile solutions of 10–20 mM peptide tended to develop a gel-like consistency over several days which was due to massive fibril formation, as detected using electron microscopy. Figure 2 shows an electron micrograph of TTR 105–115 fibrils formed in 20% acetonitrile. The fibrils were approximately 10 nm wide, of indeterminant length, and contained substructure involving several mutually twisted strands. Fibrils of the same morphology were formed by TTR 10–20 and TTR 105–115^{Met111}. X-Ray diffraction patterns showed the classical cross β-sheet pattern seen for all amyloids (16), and greeny gold birefringence was observed under polarised light in congo red stained preparations of the gel (Fig. 3).

Interestingly, NMR spectra of the samples containing gel did not display any evidence of line broadening or shifted signals. It appears that the macromolecular fibril matrix itself yields signals that are too broad to detect, and also that it does not interfere with the dynamics of the remaining monomeric species, which give rise to normal NMR spectra. These samples presumably contained reduced concentrations of monomeric peptide, but it was found that even after several months gelled samples still gave rise to well resolved spectra with little apparent reduction in intensity of the detected signals.

It was not apparent from these studies whether the rate of fibril formation differed between the three peptides. Time course studies could not be carried out using EM as a measure of fibril formation owing to limited access to this facility. It appeared that the rates of gel formation in solutions of the three peptides at similar concentrations and in the same solvent system were very similar.

^1H shift assignment

Proton chemical shifts for TTR 10–20, TTR 105–115 and TTR 105–115^{Met111} in 30% acetonitrile were assigned using TOCSY and DQF-COSY spectra to identify residue types from their side-chain connectivities. Sequential assignments were made using NOESY spectra by locating the sequential $d_{\alpha N}(i,i+1)$ and $d_{NN}(i,i+1)$ connectivities. Figure 4 shows examples of ^1H NMR spectra which demonstrate the good resolution and assignment of the connectivities.

Chemical shifts of the ^1H signals in each peptide are listed in Table 1. These were measured from DQF-COSY spectra and referenced internally against DSS which was added at the end of the experiment.

Deviation of $^1H\alpha$ shifts from random-coil chemical shifts

The $^1H\alpha$ shifts of peptides and proteins are highly sensitive to structural effects (24, 25). In particular upfield $^1H\alpha$ shifts (relative to the random coil shift for a given residue) occur for regions which are α-helical in nature (26). Downfield shifts are observed for $^1H\alpha$ in β-strand extended conformations. The deviations from random coil chemical shifts can therefore provide a preliminary indication of secondary structural elements in protein and peptides. These values for TTR 10–20, TTR 105–115 and TTR 105–115^{Met111} in 30% acetonitrile are illustrated in Fig. 5.

It can be seen that the $^1H\alpha$ shifts along the sequences of these peptides display regions of predominantly upfield shifted Hα's. The largest deviations, of about 0.3 ppm, occur for *N*-terminal residues owing to the inductive effect of the NH_3^+ group. The other deviations are smaller, averaging only 0.1 ppm. The region between residues 3–6 in TTR 105–115 and TTR 105–115^{Met111} is particularly striking, showing a gradient of upfield shifts about residue 4. Upfield deviations for the protons of TTR 10–20 occur between residues 3–9 and vary in intensity. Downfield shifts occur in all peptides for residues which precede proline, as is commonly observed (27).

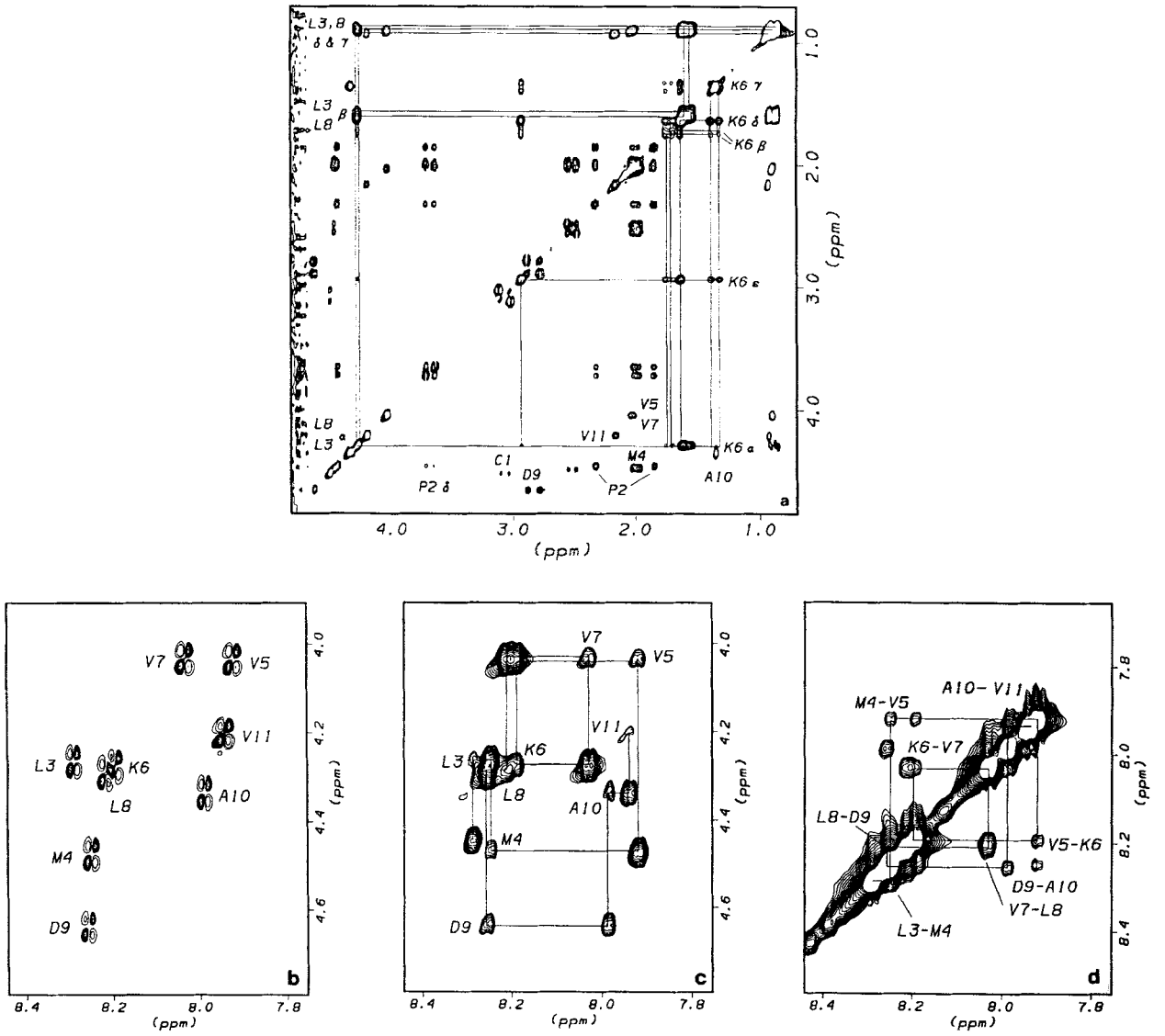

FIGURE 4

Expanded regions from ^{1}H NMR spectra of TTR 10–20 (500 MHz, 1 °C): (a) TOCSY spectrum (120 ms mixing time) showing intraresidue side-chain connectivities. Those of Leu 3, Leu 8 and Lys 6 are highlighted, and Hα–Hβ connectivities are indicated for the remaining residues. (b) NH–αH region of COSY spectrum. (c) NH–αH region of NOESY spectrum (250 ms mixing time) showing sequential connectivities. (d) NH–NH region of NOESY spectrum confirming sequential connectivities.

$^3J_{NH-\alpha H}$ *coupling constants*

$^3J_{NH-\alpha H}$ coupling constant permits a qualitative estimation of the intervening torsion angle (ϕ) between the NH and the αH. Values of about 4 Hz are often measured in regions of α-helix and 8–10 Hz in extended structures (26). For small linear peptides, however, backbone flexibility often leads to conformationally averaged values of 6–7 Hz (29). Coupling constant measurements thus tend to be less sensitive to the presence of populations of structured species than ^{1}Hα shifts or long range NOEs (29). Accordingly, coupling constants deviating from these averaged values reflect a significant population of species with a structural predisposition.

Table 2 shows the $^3J_{NH-\alpha H}$ coupling constants for the three peptides which were measured from resolved NH signals in the 1D spectrum, as well as DQF-COSY crosspeaks, adjusted for the distortion due to the overlap of antiphase peaks in such spectra (30). It may be seen that where both measurements were possible, the values were in good agreement.

The $^3J_{NH-\alpha H}$ coupling constants measured for all

TABLE 1

^1H chemical shifts[a] (ppm) for TTR 10–20, TTR 105–115 and TTR 105–115 ^{Met111} in 30% acetonitrile at 1 °C

Residue	NH	αH	βH		Others
TTR 10–20					
Cys 1	–	4.51	3.12	3.02	
Pro 2	–	4.45	2.32	1.85	γCH_2 2.01 1.97, δCH_2 3.72 3.65
Leu 3	8.29	4.27	1.61	1.56	γCH 1.56, δCH_3 0.93 0.88
Met 4	8.25	4.47	1.97	1.94	γCH_2 2.55 2.49, εCH_3 2.00
Val 5	7.92	4.03	2.02		γCH_3 0.89
Lys 6	8.20	4.28	1.77	1.70	γCH_2 1.39 1.33, δCH_2 1.64 εCH_2 2.94
Val 7	8.03	4.03	2.02		γCH_3 0.91
Leu 8	8.22	4.29	1.61	1.56	γCH 0.91, δCH_3 0.86
Asp 9	8.26	4.64	2.89	2.77	
Ala 10	7.99	4.34	1.35		
Val 11	7.95	4.20	2.15		γCH_3 0.93
TTR 105-115					
Tyr 1	–	4.26	3.13	3.03	2,6H 7.10, 3,5H 6.81
Thr 2	8.31	4.43	4.13		γCH_3 1.27
Ile 3	8.26	4.07	1.86		γCH_2 1.51 1.22 γCH_3 1.22, δCH_3 0.89
Ala 4	8.24	4.15	1.35		
Ala 5	8.01	4.19	1.37		
Leu 6	7.89	4.26	1.68	1.66	γCH 1.57, δCH_3 0.91 0.84
Leu 7	7.84	4.35	1.65	1.62	γCH 1.55, δCH_3 0.90 0.84
Ser 8	7.99	4.71	3.86	3.78	
Pro 9	–	4.35	2.11	1.52	γCH_2 1.86 1.59, δCH_2 3.70 3.62
Tyr 10	7.85	4.60	3.20	2.79	2,6H 7.10, 3,5H 6.81
Ser 11	7.89	4.45	3.95	3.87	
TTR 105–155^{met111}					
Tyr 1	–	4.27	3.12	3.04	2,6H 7.11, 3,5H 6.81
Thr 2	8.40	4.39	4.09		γCH_3 1.15
Ile 3	8.31	4.08	1.83		γCH_2 1.19 0.92, γCH_3 1.18, δCH_3 0.88
Ala 4	8.33	4.18	1.35		
Ala 5	8.13	4.20	1.35		
Leu 6	8.00	4.28	1.65	1.63	γCH 1.61, δCH_3 0.90 0.83
Met 7	8.08	4.47	2.05	1.95	γCH_2 2.57 2.49, εCH_3 2.02
Ser 8	8.16	4.72	3.86	3.81	
Pro 9	–	4.35	2.11	1.56	γCH_2 1.86 1.62, δCH_2 3.71 3.63
Tyr 10	7.92	4.60	3.17	2.81	2,6H 7.11, 3,5H 6.81
Ser 11	7.96	4.43	3.93	3.85	

[a] Relative to DSS at 0.0 ppm.

three peptides were within the limits expected for conformationally averaged species. The trend was only deviated from in the case of alanine residues. The five smallest coupling constants correspond to the five alanine NH–αH couplings in the peptides, with values between 4.8 and 6.3 Hz. This is suggestive of a trend towards a helix or turn conformation. A fully formed α-helix is unlikely to be present, since most other coupling constants show conformationally averaged values.

D_2O exchange

The exchange rate of an amide proton in peptides or proteins is related to the degree to which it is exposed to solvent. It has been shown that amide protons either participating in hydrogen-bonded secondary structure or existing in the protein interior may be detected for hours or days after dissolution in D_2O (31).

The NH exchange in linear peptides is frequently very fast due to the conformational fluctuations which typically occur. Peptides containing secondary structure may exist in equilibrium with unfolded forms, and NHs may only be observed for periods of less than 1 h. Nevertheless, relative exchange rates within this time frame can reflect regions of transient secondary structure. For this study NH signals persisting for longer than half an hour were classified as 'slow'.

D_2O exchange experiments for TTR 10–20, TTR

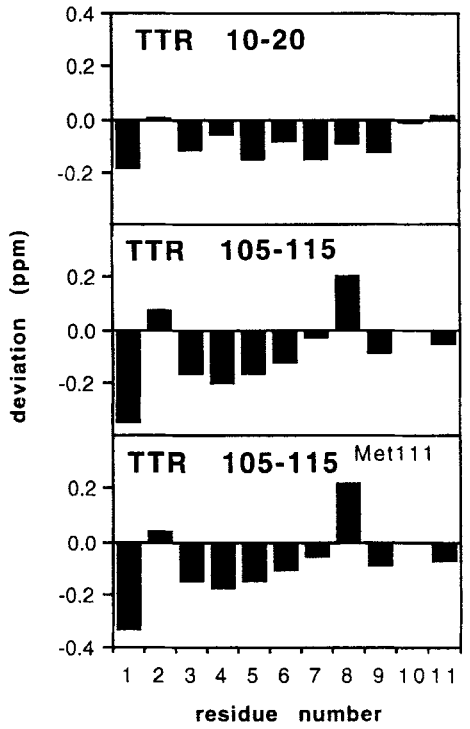

FIGURE 5

Deviation of $^1H\alpha$ chemical shifts from their random coil values (26) for the peptides TTR 10–20, TTR 105–115 and TTR 105–115^{Met111} in 30% acetonitrile, pH 3–4 and 1 °C. Differences are expressed as $\delta_{measured} - \delta_{random}$.

105–115 and TTR 105–115^{Met111} were conducted in 30% acetonitrile/D_2O at 25 °C. 1D spectra were collected at 5, 10, 20, 30 and 70 min from the time the peptide was dissolved. NH signals which were not overlapped could be ranked in order of their rate of exchange. For each peptide a TOCSY spectrum was recorded, 30 min after dissolution, to identify unambiguously those NH signals lasting longer than 30 min.

TTR 105–115 1D and TOCSY D_2O exchange spectra are illustrated in Figs. 6 and 7. It was clear that the T2 NH exchanged extremely rapidly, not being observed even at 5 min. All other NH peaks were overlapped, so that their relative exchange rates could not be determined. The TOCSY experiment run between 35 and 65 min, however, showed unambiguously that NHs of L6, L7 and S8 as well as Y10 persisted for longer than 30 min. It was interesting that the slower exchanging NHs occurred in consecutive sites towards the *C*-terminus of the peptide, with the exception of the interruption by P9 NH.

A similar analysis of TTR 105–115^{Met111} revealed that the T2 signal disappeared most quickly, with nearly no signal apparent after 10 min (Fig. 6). I3 and A4 exchanged quite quickly, and were not visible in the 1D spectrum after 30 min. L6 and Y10 were the slowest exchanging signals, remaining visible in the TOCSY spectrum run between 35 and 65 min.

It is interesting to compare residues 6 to 10 in TTR 105–115^{Met111} and TTR 105–115. Whilst L6 and Y10 NHs exchanged slowly in both peptides, S8 and residue 7 were only visible in the TTR 105–115 TOCSY spectrum. The difference may be attributable to the methionine substitution at position 7 in TTR 105–115^{Met111} under these otherwise almost identical conditions. It appears that some property of the methionine-containing derivative resulted in reduced protection of the residue 7 and 8 NH sites of the peptide relative to those in TTR 105–115.

The TTR 10–20 1D spectrum run after 5 min showed strong NH signals, several of which were overlapped.

TABLE 2

$^3J_{NH-\alpha H}$ coupling constants (Hz) measured for peptides TTR 10–20, TTR 105–115 and TTR 105–115^{Met111} from both 1D (25 °C) and DQF-COSY spectra (1 °C)

Residue	TTR 10–20		TTR 105–115		TTR 105–115^{Met111}	
	1D	COSY	1D	COSY	1D	COSY
2	[a]	[a]	[b]	7.4	[b]	7.5
3	6.6	6.6	[b]	6.7	7.3	6.9
4	7.3[c]	7.0	4.7[c]	4.8	5.0	4.9
5	7.4	7.4	6.0[c]	6.3	5.6	5.5
6	[b]	6.7	7.5	7.2	7.1[c]	7.6
7	7.7	7.9	7.1	7.5	7.5	8.0
8	[b]	5.5	6.0[c]	6.5	6.6	6.6
9	7.3[c]	7.3	[a]	[a]	[a]	[a]
10	5.9	5.8	[b]	7.4	8.3	7.9
11	7.7	7.4	[b]	7.4	7.1[c]	7.7

[a] Position of proline in sequence.
[b] Overlapped NH signal in 1D spectrum.
[c] Approximate value from partially overlapped NH signal in 1D spectrum.

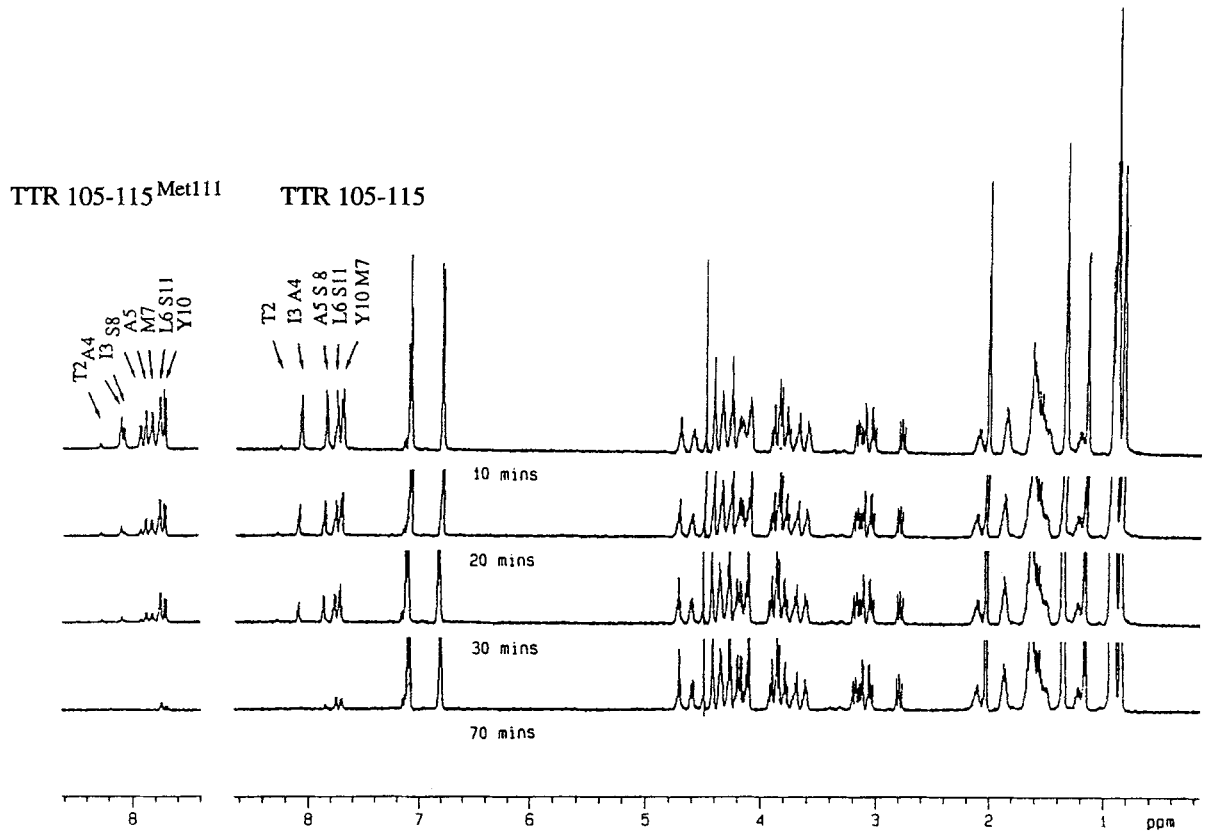

FIGURE 6

1D spectra of TTR 105–115, and the NH region of equivalent spectra of TTR 105–115^{Met111}, at various times after dissolution in 30% acetonitrile/D_2O (500 MHz, 25 °C).

Fast exchange peaks included M4 and D9 NHs. The TOCSY experiment run between 35 and 65 min identified the slowest exchanging NHs as L8, V5, K6 and V7.

Figure 8 summarises the NH sites displaying 'slow' exchange for the three peptides. The regions containing these sites tended to be near the *C*-terminus for all three peptides. These positions of the 'slow' exchange NHs

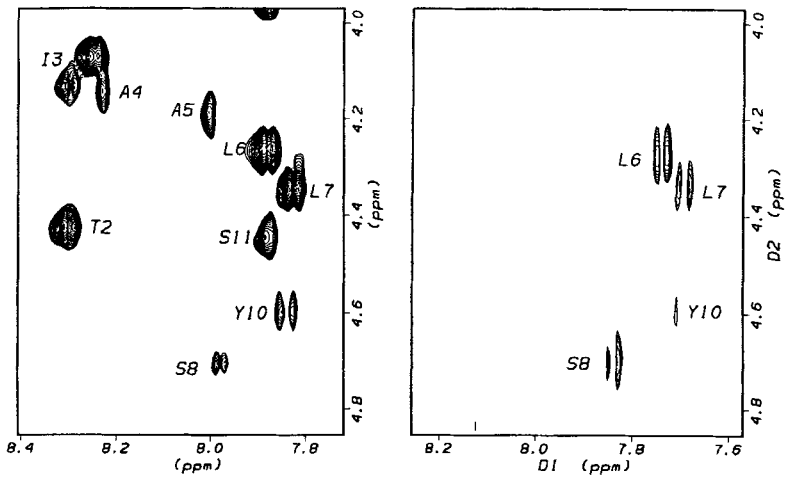

FIGURE 7

TOCSY spectra of the fingerprint region of TTR 105–115 showing (a) all the NH–αH connectivities seen in water spectra and (b) crosspeaks of 'slow' exchange NHs 30 min after dissolution in 30% acetonitrile/D_2O (500 MHz, 25 °C).

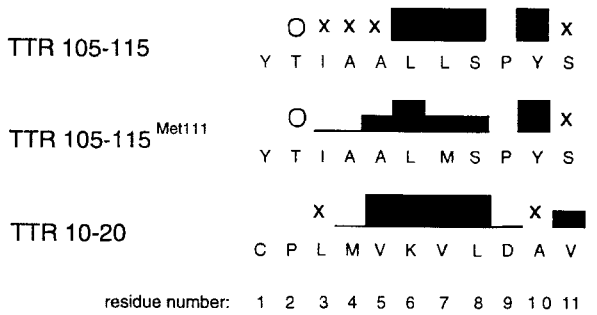

FIGURE 8

Summary of NH exchange rates observed for TTR 10–20, TTR 105–115 and TTR 105–115^{Met111}. NH signals apparent in the TOCSY spectrum run after 30 min are marked by ■. Intermediate NH exchange rates noted for resolved signals in the 1D spectra are classified as moderate (▬), fast (—) and very fast exchange (○). Signals that could not be ranked due to overlap in the 1D spectrum are marked (×).

TABLE 3

Temperature coefficients (ppb/K) measured for TTR 10–20, TTR 105–115 and TTR 105–115^{Met111}

Residue	TTR 10–20	TTR 105–115	TTR 105–115^{Met111}
2	[a]	5.7	5.2
3	5.2	6.3	6.3
4	[b]	6.6	6.1
5	6.1	6.6	6.5
6	5.9	[b]	5.8
7	5.6	[b]	6.1
8	[b]	6.9	6.1
9	5.4	[a]	[a]
10	5.1	5.7	5.2
11	6.5	[b]	4.2

[a] Indicates proline (no NH).
[b] Indicates NH signal overlap.

are consistent with H-bonding to carbonyl groups four residues prior in the sequence, as occurs within an α-helical structure. Alternatively, H-bonding within sub-populations of β-turns or steric or hydrophobic interactions of side chains could result in the observed protection of these NH sites from solvent.

NH temperature coefficients

The NH temperature coefficient, defined as the rate of change of chemical shift with temperature in ppb/K, is frequently used as a measure of NH solvent accessibility (29). Values of <3 may be observed when the NH is involved in intramolecular H-bonding (32). The observation of high temperature coefficients, however, does not preclude the possibility of there being H-bonding (33, 34). It was thus of interest to see whether the temperature coefficients for these peptides would provide any evidence of H-bonding in support of the evidence provided by D_2O exchange studies.

The NH chemical shifts for all three peptides varied linearly with temperature and the temperature coefficients determined for TTR 10–20, TTR 105–115 and TTR 105–115^{Met111} are shown in Table 3. It can be seen that values above 5 ppb/K are most commonly observed for all three peptides. The only exception is the temperature coefficient measured for S11 of TTR 105–115^{Met111}. Thus, this NH may in some way be more protected from solvent, though a reason for this lone case is not obvious.

There is no overall reflection of the higher degree of NH protection towards the *C*-termini of the peptides as indicated by D_2O exchange studies. This is, perhaps, not surprising since the D_2O exchange studies, which

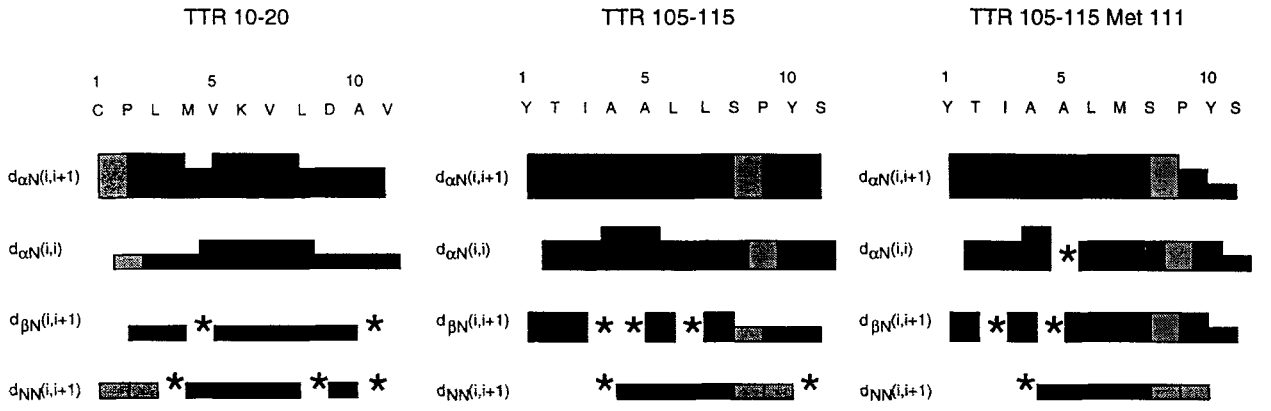

FIGURE 9

Summary of NOE connectivities measured for peptide (a) TTR 10–20, (b) TTR 105–115 and (c) TTR 105–115^{Met111} (30% acetonitrile, 500 MHz 1 °C). The intensities of the NOE crosspeaks are indicated by the thickness of the line, grouped into strong, medium and weak. Overlapping, and therefore ambiguous crosspeaks are indicated by *. Connectivities not expected to be present due to the lack of the specified protons (*i.e.* Pro NH) are shaded.

would be expected to be more sensitive for the detection of slow exchange, indicated that all NH exchange rates were relatively fast (compared with those of larger structured species).

NOESY connectivities

Chemical shift measurements, $^3J_{NH-\alpha H}$ coupling constants, temperature coefficients and D_2O exchange rates aid the identification of regions of structural propensity; however, NOE connectivities are necessary for the confirmation and more precise description of a structured form (29).

The sequential and intraresidue NOEs observed for the three peptides are summarised in Fig. 9. The observation of $d_{NN}(i,i+1)$ NOE connectivities indicates the presence of a population of structures containing helix or turn. Their weak intensity, however, compared with the corresponding $d_{\alpha N}(i,i+1)$ connectivities suggests that a helix may only exist for a low percentage of the conformers (35). Likewise, the observation of strong $d_{\alpha N}(i,i+1)$ intensities relative to those of $d_{\alpha N}(i,i)$ connectivities indicates that the peptides also have some population of extended or random forms, particularly TTR 10–20, for which weaker $d_{\alpha N}(i,i)$ signals were observed (28).

No medium- or long-range connectivities that would demonstrate the presence of a long-lived stable helix were detected for any of the three peptides. This indicates that although the peptides may show some characteristics of helix, the structure are likely to be fluctuating between turn, helix and random forms.

DISCUSSION

These studies showed that in solution TTR 10–20, TTR 105–115 and TTR 105–115^{Met111} are comprised predominantly of random-coil structures, but may include a low percentage of turn or helical elements. The peptides displayed no predisposition to exclusively form β-strand structures in solution, as may have been supposed from the β-sheet based fibril structures they form.

A similar situation has been reported for the β-peptide of Alzheimer's disease for which a helix-sheet transition is thought to occur as the fibril forms (36). Likewise the Prion protein and insulin both contain helix prior to incorporation into the amyloid-like fibril (13, 37). No fibril-forming peptide has yet been shown to possess an intrinsic extended propensity in solution. The mechanism for fibril formation, therefore, may involve the induction of β-extended form as the monomer interacts with the aggregate. Alternatively, it is possible that structures other than classical β-sheet may be present in some forms of amyloid, but the predominant view, derived from CD, FTIR and X-ray data, is that the fibrils are β-sheet based (9).

The TTR fragments examined in this study displayed very similar characteristics to one another, so that the above conclusions apply to all three peptides. It appeared, however, that TTR 10–20 displayed the least turn or helix tendency (based on the relatively weak $d_{\alpha N}(i,i)$ NOEs observed and less uniformly upfield shifted $^1H\alpha$ shifts). TTR 105–115, on the other hand, appeared to posses a greater turn or helix propensity than TTR 105–115^{Met111} based on the greater number of 'slow' exchange NH's recorded. The Met substitution in TTR may contribute to the amyloidogenicity of this mutant through a decreased tendency to turn.

ACKNOWLEDGMENTS

We thank Barry Veitch (Department of Biochemistry, Monash University) for providing electron micrographs of the fibrils, and Dr. Matthew Wilce (St. Vincent's Institute of Medical Research) for the polarised light micrographs.

REFERENCES

1. Blake, C.C.F. & Oatley, S.J. (1977) *Nature (London)* **268**, 115–120
2. Colon, W. & Kelly, J.W. (1992) *Biochemistry* **31**, 8654–8660
3. Westermark, P., Sletten, K., Johansson, B. & Cornwell, G.G. (1990) *Proc. Natl. Acad. Sci. USA* **87**, 2843–2845
4. Benson, M.D. (1989) *Trends Neurosci.* **12**, 88–92
5. Kisilevsky, R. (1987) *Can. J. Physiol. Pharmacol.* **65**, 1805–1815
6. (1192) in *Amyloid and Amyloidosis* (Natvig, J.B., Forre, O., Husby, G., Husebekk, A., Skogen, B., Sletten, K. & Westermark, P., eds.) Kluwer Academic Publishers, Dordrecht
7. Kirschner, D.A., Abraham, C. & Selkoe, D.J. (1986) *Proc. Natl. Acad. Sci.* **83**, 503–507
8. Halverson, K., Fraser, P.E., Kirschner, D.A. & Lansbury Jr., P.T. (1990) *Biochemistry* **29**, 2693–244
9. Lansbury, Jr., P.T. (1992) *Biochemistry* **31**, 6865–6870
10. Barrow, C.J., Yasuda, A., Kenny, P.T.M. & Zagorski, M.G. (1992) *J. Mol. Biol.* **225**, 1075–1093
11. Jarret, J.T., Berer, E.P. & Lansbury Jr., P.T. (1993) *Biochemistry* **32**, 4693–4697
12. Fraser, P.E., Nguyen, J.T., Inouye, H., Surewicz, W.K., Selkoe, D.J., Podlisny, M.B. & Kirschner, D.A. (1992) *Biochemistry* **31**, 10716–10723
13. Gasset, M., Baldwin, M.A., Fletterick, R.J. & Prusiner, S.B. (1993) *Proc. Natl. Acad. Sci.* **90**, 1–5
14. Safer, J., Roller, P.P., Gajdusek, C. & Gibbs Jr., C.J. (1993) *J. Biol. Chem.* **268**, 20276–20284
15. Gustavsson, A., Engstrom, U. & Westermark, P. (1991) *Biochem. Biophys. Res. Commun.* **175**, 1159–1164
16. Jarvis, J., Craik, D.J. & Wilce, M.C.J. *Biochem. Biophys. Res. Commun.* **192**, 991–998
17. Kraulis, P.J. (1991) *J. Appl. Crystallogr.* **24**, 946–950
18. Nordlie, M., Sletten, K., Husby, G. & Ranlov, P.J. (1988) *Scand. J. Immunol.* **27**, 119–122
19. Prusiner, S.B., McKinley, M.P., Bowman, K.A., Bolton, D.C., Bendheim, P.E., Groth, D.F. & Glenner, G.G. (1983) *Cell* **35**, 349–358
20. Marion, D. & Wuthrich, K. (1983) *Biochem. Biophys. Res. Commun.* **113**, 967–974
21. Bax, A. & Davis, D.G. (1985) *J. Magn. Reson.* **65**, 335–360
22. Rance, M., Sorenson, O.W., Bodenhausen, G., Wagner, G., Ernst, R.R. & Wuthrich, K. (1983) *Biochem. Biophys. Res. Commun.* **117**, 479–495
23. Plateau, P. & Gueron, M. (1982) *J. Am. Chem. Soc.* **104**, 7310–7311

24. Wishart, D.S., Sykes, B.D. & Richards, F.M. (1991) *J. Mol. Biol.* **222**, 311–333
25. Wishart, D.S., Sykes, B.D. & Richards, F.M. (1992) *Biochemistry* **31**, 1647–1651
26. Wüthrich, K. (1986) in *NMR of Proteins and Nucleic Acids*, Wiley & Sons, New York
27. Howarth, O.W. & Lilley, D.M. (1978) *Progr. NMR Spectrosc.* **12**, 1–40
28. Dyson, H.J., Rance, M., Houghten, R.A., Wright, P.E. & Lerner, R.A. (1988) *J. Mol. Biol.* **210**, 201–217
29. Dyson, H.J. & Wright, P.E. (1991) *Annu. Rev. Biophys. Chem.* **20**, 519–538
30. Neuhaus, D., Wagner, G., Vašák, M., Kägi, J.H.R. & Wüthrich, K. (1985) *Eur. J. Biochem.* **151**, 257–273
31. Englander, S.W. & Kallenbach, N.R. (1983) *Ann. Rev. Biophys.* **16**, 521–655
32. Hruby, V. (1974) in *Chemistry and Biochemistry of Peptides* (Weinstein, B., ed.) Marcel Dekker Inc. New York, Vol. 3 p. 1
33. Andersen, N.H., Chen, C., Marschner, T.M., Krystek Jr., S.R. & Bassolino, D.A. (1992) *Biochemistry* **31**, 1280–1295
34. Reed, J., Hull, W.E., Lieth, C.-W., Kühler, D., Suhai, S. & Kinzel, V. (1988) *Eur. J. Biochem.* **178**, 141–154
35. Bradley, E.K., Thomason, J.F., Cohen, F.E., Kosen, P.A. & Kuntz, I.D. (1990) *J. Mol. Biol.* **215**, 607–622
36. Zagorski, M.G. & Barrow, C.J. (1992) *Biochemistry* **31**, 5621–5631
37. Glenner, G.G., Eanes, E.D., Bladen, H.A., Linke, R.P. & Termine, J.D. (1974) *J. Histochem. Cytochem.* **22**, 1141–1158

Address:

David J. Craik
School of Pharmaceutical Chemistry
Victorian College of Pharmacy
Monash University
381 Royal Parade
Parkville, Victoria 3052
Australia

Tel: 6139039617
Fax: 6139032582